BIOCHEMISTRY
including biophysical chemistry & molecular biology

Article

pubs.acs.org/biochemistry

# Steady-State Kinetics and Spectroscopic Characterization of Enzyme−tRNA Interactions for the Non-Heme Diiron tRNA-Monooxygenase, MiaE

Bishnu P. Subedi, Andra L. Corder, Siai Zhang, Frank W. Foss, Jr., and Brad S. Pierce*

Department of Chemistry and Biochemistry, College of Sciences, The University of Texas at Arlington, Arlington, Texas 76019, United States

Supporting Information

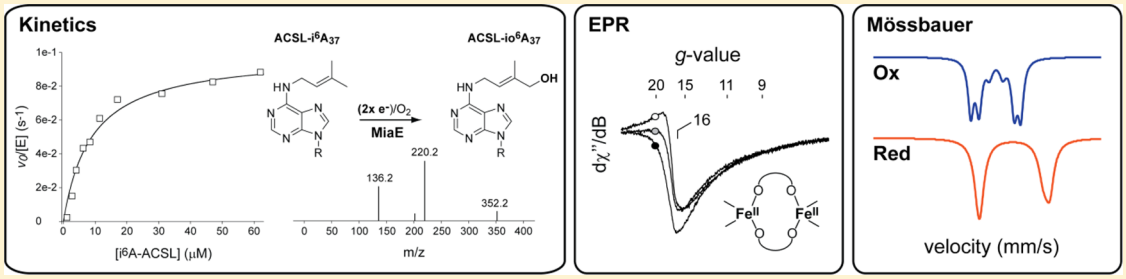


**ABSTRACT:** MiaE [2-methylthio-$N^6$-isopentenyl-adenosine(37)-tRNA monooxygenase] isolated from *Salmonella typhimurium* is a unique non-heme diiron enzyme that catalyzes the $O_2$-dependent post-transcriptional allylic hydroxylation of a hypermodified nucleotide ($ms^2i^6A_{37}$) at position 37 of selected tRNA molecules to produce 2-methylthio-$N^6$-(4-hydroxyisopentenyl)-adenosine(37). In this work, isopentenylated tRNA substrates for MiaE were produced from small RNA oligomers corresponding to the anticodon stem loop (ACSL) region of $tRNA^{Trp}$ using recombinant MiaA and dimethylallyl pyrophosphate. Steady-state rates for MiaE-catalyzed substrate hydroxylation were determined using recombinant ferredoxin (Fd) and ferredoxin reductase (FdR) to provide a catalytic electron transport chain (ETC) using NADPH as the sole electron source. As with previously reported peroxide-shunt assays, steady-state product formation retains nearly stoichiometric (>98%) *E* stereoselectivity. MiaE-catalyzed $i^6A$-$ACSL^{Trp}$ hydroxylation follows Michaelis−Menten saturation kinetics with $k_{cat}$, $K_M$, and $V/K$ determined to be 0.10 ± 0.01 $s^{-1}$, 9.1 ± 1.5 μM, and ∼11000 $M^{-1}$ $s^{-1}$, respectively. While vastly slower, MiaE-catalyzed hydroxylation of free $i^6A$ nucleoside could also be observed using the (Fd/FdR)−ETC assay. By comparison to the $V/K$ determined for $i^6A$-ACSL substrates, an ∼6000-fold increase in enzymatic efficiency is imparted by $ACSL^{Trp}$−MiaE interactions. The impact of substrate tRNA−MiaE interactions on protein secondary structure and active site electronic configuration was investigated using circular dichroism, dual-mode X-band electron paramagnetic resonance, and Mössbauer spectroscopies. These studies demonstrate that binding of tRNA to MiaE induces a protein conformational change that influences the electronic structure of the diiron site analogous to what has been observed for various bacterial multicomponent diiron monooxygenases upon titration with their corresponding effector proteins. These observations suggest that substrate−enzyme interactions may play a pivotal role in modulating the reactivity of the MiaE diiron active site. Moreover, the simplified monomeric (α) protein configuration exhibited by MiaE provide an unparalleled opportunity to study the impact of protein−effector interactions on non-heme diiron site geometry and reactivity.

To date, nearly 90 post-transcriptional modifications of transfer RNA (tRNA) have been identified across all phylogenic domains of life (Archaea, Bacteria, and Eukarya).[1,2] These modifications are made to structurally diversify tRNA, resulting in altered function and interactions with amino acids and the ribosomal machinery.[3] In many instances, the physiologic role of such modifications is unclear; however, several examples have been identified to suggest that the presence of modified nucleotides in tRNA can impact aminoacyl-tRNA selection, decrease translational frame-shifting, regulate central metabolism (citric acid cycle and thiamine biosynthesis), and initiate genes involved in bacterial virulence.[1,4] As the ribosomal machinery has historically proven to be an effective target for the development of anticancer, antibiotic, and antiviral agents, the characterization of enzymes involved in nucleotide transformations represents a rich area of mechanistic study with a great potential impact on human health.[5−8]

Within the anticodon stem loop (ACSL) of tRNA, nucleotide modifications are frequently observed at position 34 (the wobble position) or position 37 (3′ adjacent to the anticodon).[9,10] In some instances, modifications employ

**Received:** September 26, 2014
**Revised:** November 20, 2014
**Published:** December 2, 2014





DOI: 10.1021/bi5012207
*Biochemistry* 2015, 54, 363−376

**Scheme 1. Hypermodification Enzyme Pathway for 2-Methylthio-$N^6$-(4-hydroxyisopentenyl)-adenosine ($ms^2io^6A_{37}$) Synthesis**

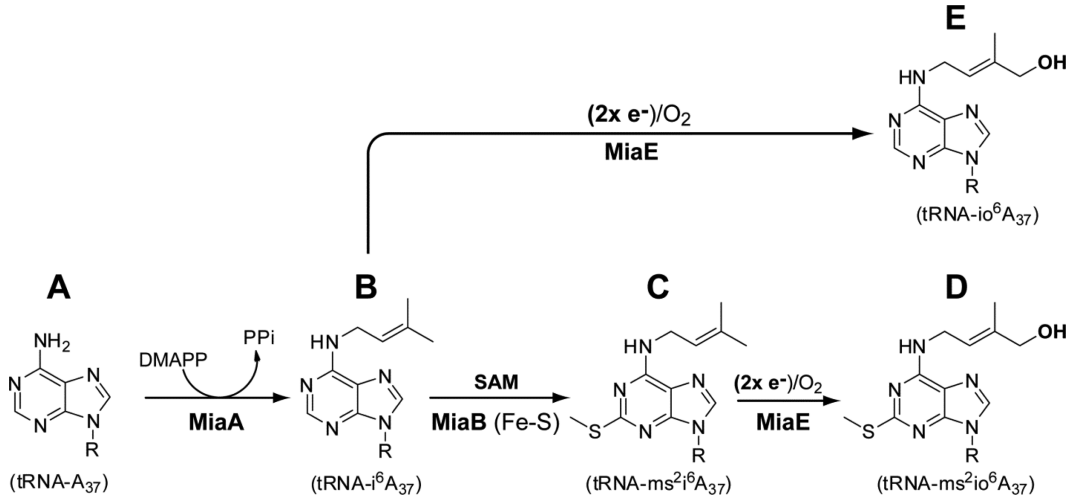


multiple enzymes within a complex biochemical pathway to produce hypermodified nucleotides. For instance, nearly all eukaryotic and bacterial tRNAs that read codons starting with U are modified by the enzymes MiaA and MiaB as illustrated in Scheme 1. In the first step, dimethylallyl ($\Delta^2$-isopentenyl) diphosphate-tRNA transferase (EC 2.5.1.8, designated MiaA) catalyzes the nucleophilic substitution of the dimethylallyl group from dimethylallyl pyrophosphate (DMAPP) to the exocyclic 6-amino nitrogen of $A_{37}$ ($N^6$) to yield $N^6$-isopentenyl-adenosine ($i^6A_{37}$) with release of inorganic pyrophosphate.[11] The second enzymatic transformation involves the formal methylthiolation of $i^6A_{37}$ at the C2 position to produce 2-methylthio-$N^6$-isopentenyl-adenosine ($ms^2i^6A_{37}$). The enzyme that catalyzes this remarkable transformation (2-methylthio-$N^6$-isopentenyl-adenosine synthase, designated MiaB) requires *S*-adenosylmethionine as a cosubstrate and is a member of the radical *S*-adenosylmethionine (SAM) methylthiotransferase family of enzymes.[12−14] With the notable exception of $tRNA_{I,V}^{Ser(GGA)}$, nearly all eukaryotic and bacterial tRNAs that read codons starting with U contain the $ms^2i^6A$ modification.[2,15]

While absent in eukaryotes, some facultative bacteria use a non-heme diiron enzyme [MiaE, 2-methylthio-$N^6$-isopentenyl-adenosine(37)-tRNA monooxygenase] to catalyze the $O_2$-dependent hydroxylation of $ms^2i^6A_{37}$ to produce 2-methylthio-$N^6$-(4-hydroxyisopentenyl)-adenosine ($ms^2io^6A_{37}$).[16] While MiaE can utilize $i^6A_{37}$ as a substrate, whole cell assays suggest a preference for $ms^2i^6A_{37}$.[17−19] As previously mentioned, MiaA and MiaB are common in both eukaryotes and prokaryotes; by contrast, MiaE is found within only a small subset of facultative anaerobic bacteria such as *Salmonella typhimurium*.[20] It has been postulated that within these bacteria the extent of $A_{37}$ hydroxylation is involved in regulating aromatic amino acid uptake, enterochelin synthesis, iron transport, and aerobiosis.[4,15,20−22]

MiaE is a member of the non-heme diiron family of enzymes.[16,22,23] Other members of this family include the hydroxylase components of the bacterial multicomponent monooxygenases (BMMs) [methane monooxygenase (MMOH) and toluene monooxygenase (ToMOH)], the small subunit of ribonucleotide reductase (R2), and stearoyl-acyl carrier protein $\Delta^9$-desaturase ($\Delta$9D).[24−26] This incredibly diverse family of enzymes has been identified all throughout the biological kingdom, and its members are capable of catalyzing an impressive array of chemical oxidations (mono- and dioxygenations and aliphatic desaturation).[26] Remarkably, despite accommodating a broad spectrum of substrates, the first coordination sphere of the diiron active site is essentially conserved among non-heme diiron oxidase/oxygenase enzymes.

The typical quaternary protein structure observed in non-heme diiron enzymes is multimeric.[27] Indeed, among the hydroxylase components of bacterial multicomponent monooxygenase (BMM) enzymes, a noncovalent heterotrimeric dimer complex $(\alpha\beta\gamma)_2$ is the most frequently observed protein configuration.[28] By contrast, the simplest quaternary structure reported for non-heme diiron enzymes is homodimeric ($\alpha_2$). For instance, both the small subunit of ribonucleotide reductase (R2) and stearoyl-acyl carrier protein (18:0-ACP) $\Delta^9$-desaturase ($\Delta$9D) exhibit a homodimeric protein configuration in which each protomer contains a diiron active site.[24−26] Perhaps coincidentally, it has been reported that both $\Delta$9D and R2 exhibit properties consistent with "half-sites" reactivity, implying that the two protomers of these homodimeric enzymes do not act independently during catalysis.[29−32] For example, rapid-mix/chemical quench experiments with $\Delta$9D demonstrate the most compelling evidence for "half-sites" reactivity within a non-heme diiron enzyme. In these reactions, the prereduced enzyme−substrate complex ($\Delta$9D:18:0-ACP) was rapidly mixed with $O_2$-saturated buffer prior to chemical quenching at selected time points. Formation of the observed product (18:1-ACP) followed two distinct kinetic phases, an initial "burst phase" ($k_{burst} \sim 95\ s^{-1}$) followed by a second linear phase ($k_{linear} \sim 4\ s^{-1}$).[33] As $\Delta$9D is a homodimer, each protomer has an equivalent diiron site capable of generating product, and thus, the expected amplitude of this burst phase should be twice the protein concentration. Remarkably, the observed amplitude in these experiments was roughly equivalent to one product (18:1-ACP) generated per $\Delta$9D homodimer. On the basis of these experiments, it was concluded that the two active sites within $\Delta$9D are not simultaneously catalytically active.

In stark contrast to the multimeric protein configuration exhibited by all other non-heme diiron monooxygenases, MiaE exhibits a monomeric ($\alpha$) protein configuration (one active site within a single protomer) as indicated by size exclusion



DOI: 10.1021/bi5012207
*Biochemistry* 2015, 54, 363−376

chromatography[16] and analytical ultracentrifugation.[23] To the best of our knowledge, this is the first example of a monomeric non-heme diiron oxygenase/oxidase. Therefore, this enzyme provides an unprecedented opportunity to study a minimal non-heme diiron enzyme in the absence of any potential for interprotomer cooperativity.

In this work, the steady-state kinetics of MiaE-catalyzed tRNA hydroxylation and the impact of protein−tRNA interactions on kinetics, protein secondary structure, and active site electronic configuration were characterized using circular dichroism (CD), parallel mode electron paramagnetic resonance (EPR), and Mössbauer spectroscopy. Remarkably, the $g \sim 16$ parallel mode EPR signal of the reduced enzyme shifts upon binding of RNA oligomers corresponding to the ACSL region of MiaE tRNA substrates. This spectroscopic shift is remarkably similar to what has been previously reported for the reduced bacterial multicomponent diiron monooxygenases upon titration with their corresponding effector proteins.[34−39] These spectroscopic results provide scaffolding for a more in-depth investigation of this enzyme. Furthermore, given the simplified monomeric ($\alpha$) protein configurations exhibited by MiaE, characterization of this enzyme represents an unprecedented opportunity to study the impact of protein−effector interactions on non-heme diiron site geometry and reactivity.

## MATERIALS AND METHODS

**Cloning of MiaA.** The *miaA* gene was isolated from *Salmonella enterica* strain LT2 genomic DNA (ATCC 700720) using primers purchased from Integrated DNA Technologies (https://www.idtdna.com). A two-step polymerase chain reaction (PCR) amplification was used to isolate the open reading frame from genomic DNA and incorporate restriction sites (SgfI and PmeI) for Flexi-vector cloning (Promega, Madison, WI), followed by insertion of a recognition site for tobacco etch virus protease (TEV). First, (miaA specific) PCR primers: forward 5′-(AAC CTG TAC TTC CAG TCC AAT GAT GTA AGC AAG GCG AGC CTG)-3′ and reverse 5′-(GCT CGA ATT CGT TTA AAC TAG TCT GCG ATA GCA CCA ACA ACC)-3′. Second, (TEV site insertion) primers: forward 5′-(GGT TGC GAT CGC CGA AAA CCT GTA CTT CCA GTC C)-3′ and reverse 5′-(GTG TGA GCT CGA ATT CGT TTA AAC)-3′. The DNA produced by this two-step PCR amplification was cloned into an IPTG-inducible T7 vector (designated pVP80K) as described previously for the MiaE expression vector.[23] Sequence verification of *miaA* was performed by Sequetech (Mountain View, CA, http://sequetech.com/). The resulting plasmid expresses an N-terminal fusion of maltose binding protein (MBP) and MiaA.

**Enzyme Purification.** *MiaA Expression and Purification.* The MiaA expression vector (pMIAAK) was transformed into competent BL21(DE3) *Escherichia coli* cells (Novagen) by heat shock and was grown overnight on a LB medium agar plate containing 25 $\mu$g/mL kanamycin (Kan) at 37 °C. The following day, a single colony was selected for growth in liquid LB (Kan) medium for training on antibiotic prior to inoculation of a 10 L BF-110 fermentor (New Brunswick Scientific) at 37 °C. Cell growth was followed by optical density at 600 nm ($OD_{600}$). Induction was initiated by addition of 0.5 mM IPTG and 20 g of casamino acids at an $OD_{600}$ of ∼4. Upon induction, the temperature of the bioreactor was decreased from 37 to 25 °C and agitation was set to maintain an $O_2$ concentration of 20% relative to air-saturated medium. After 4h induction, the cells were pelleted by centrifugation (Beckman-Coulter Avanti J-E, JA 10.5 rotor) at 18600×*g* for 15 min, and the paste was stored at −80 °C. Confirmation of MiaA expression was performed by sodium dodecyl sulfate−polyacrylamide gel electrophoresis (SDS−PAGE) of lysed cells before and after IPTG induction. In a typical MiaA purification, ∼10 g of frozen cell paste was thawed on ice in a lysis buffer [20 mM HEPES and 100 mM NaCl (pH 8.0)] along with 10 $\mu$g/mL each lysozyme, deoxyribonuclease I, and ribonuclease. Once thawed, the cell suspension was sonicated with a 30 s on/off pulse cycle for a total time of 10 min. The resulting slurry was then centrifuged at 4 °C (48000×*g*) for 1 h. Following centrifugation, the supernatant was decanted from the pellet and then loaded onto a pre-equilibrated amylose column (NEB, 13.0 cm × 3.5 cm). Unbound protein and impurities were washed from the column by addition of 100 mL of the pre-equilibration/wash buffer [20 mM HEPES, 300 mM NaCl, and 0.3 mM tris(2-carboxyethyl)-phosphine (TCEP) (pH 8.0)]. Elution of the MBP−MiaA fusion protein was performed by addition of 3 column volumes of maltose buffer [20 mM HEPES, 300 mM NaCl, 20 mM maltose, and 0.3 mM TCEP (pH 8.0)]. Recovered protein was concentrated with an Amicon/$N_2$ stir cell equipped with an Ultracel 30 kDa ultrafiltration membrane (Millipore). The MBP affinity tag was removed by overnight TEV protease cleavage as described elsewhere.[23] The protein purity and concentration were confirmed by SDS−PAGE and the Bradford protein assay, respectively.

*TEV Protease Purification and Reaction Conditions.* Tobacco etch virus (TEV) protease was purified through a Ni-IMAC column as described previously.[23] MBP fusion proteins were cleaved at 4 °C with TEV protease (5:1 ratio based on absorbance at 280 nm) in HEPES buffer [20 mM HEPES, 100 mM NaCl, and 0.3 mM TCEP (pH 8.0)].

*MiaE Expression and Purification.* Protocols for MiaE expression, purification, and cleavage from MBP fusion protein are described in detail elsewhere.[23] The $^{57}$Fe-enriched MiaE protein was prepared for Mössbauer study by growing the MiaE vector in M9 medium in which $^{57}$Fe was used as the only iron source during growth and expression of bacteria. The purity and concentration of MiaE protein were determined by UV−visible spectroscopy ($A_{280}/A_{370} \sim 7.8$).

*Ferredoxin (Fd).* *Anabaena* vegetative [2Fe-2S] ferredoxin was expressed and purified as described elsewhere.[40,41] Briefly, cell free extract was loaded onto a DEAE anion exchange column pre-equilibrated in 20 mM HEPES and 50 mM NaCl (pH 8.0). Protein was eluted using a NaCl gradient (50 to 400 mM) at pH 8. The purity of the protein was confirmed via both SDS−PAGE analysis and UV−visible spectroscopy. The protein concentration was determined using the known molar extinction coefficient ($\varepsilon_{420}$ = 9700 $M^{-1}$ $cm^{-1}$). The ferredoxin expressing T7 IPTG-inducible vector was a generous gift from B. G. Fox (Department of Biochemistry, University of Wisconsin, Madison, WI).

*Ferredoxn NADP$^+$ Reductase (FdR).* Spinach FdR was purchased from Sigma-Aldrich (CAS Registry No. 9029-33-8) and reconstituted to the desire concentration in 20 mM Tris buffer (pH 8.0) before use.

*Anticodon Stem Loop (ACSL) of tRNA.* Small 17-nucleotide RNA oligomers corresponding to the anticodon stem loop of *S. typhimurium* were purchased from Integrated DNA Technology (idtdna.com). The sequence and designation for each RNA oligomer used in these experiments are as follows: ACSL$^{Trp}$, [$^{27}$CCGGUCUCCAAAACCG$^{43}$G]; ACSL$^{Leu}$, [$^{28}$GUUGAUUCAAAAUCAA$^{44}$C]; ACSL$^{Met}$, [$^{28}$CAUCACUCAUAAUG-



DOI: 10.1021/bi5012207
*Biochemistry* 2015, 54, 363−376

AU[44]G]. For the sake of clarity, the A targeted for MiaA and MiaE modification ($A_{37}$) is shown in bold and underlined. For control experiments, a single-stranded 10-nucleotide RNA oligo sequence (GGCUACGUAG) was employed (termed ssRNA). This sequence lacks the ability to form a hairpin loop and thus represents a control for adventitious binding of single-stranded RNA. All lyophilized RNA oligomers were reconstituted in buffer [30 mM HEPES, 100 mM KCl, 2 mM $MgCl_2$, and 50 mM ammonium acetate (pH 7.0)]. The final concentration for each RNA solution was based on the exact mass of the RNA oligomer reported by IDT quality assurance and separately confirmed with a NanoDrop UV−visible spectrophotometer (Thermo Scientific). To ensure homogeneous folding of RNA into a stable hairpin loop, solutions of RNA oligomers were temperature-annealed as described previously.[42] Briefly, a PCR thermal cycler (MJ mini gradient, Bio-Rad) was utilized to increase the temperature of RNA solutions (25−50 μL) to 95 °C over the course of 2 min. After 1 s at 95 °C, solutions were then cooled to 4 °C over the course of 35 min. RNA secondary structure was confirmed by a CD J-715 spectropolarimeter (JASCO Inc., Easton, MD).

**MiaA Activity Assay.** Approximately 6 μM $ACSL^{Trp}$ was annealed and treated with 200 nM MiaA, 100 μM dimethyl allyl pyrophosphate (DMAPP), and 100 μg of bovine serum albumin (BSA) in 1 mL of TMD buffer [60 mM Tris-HCl, 20 mM $MgCl_2$, and 2 mM DTT (pH 7.5)] at ambient temperature (22 ± 2 °C) to isopentenylate the A37 within the $ACSL^{Trp}$ sequence. For kinetic studies, sample aliquots were removed at selected time points (1−60 min), heat-denatured at 95 °C for 2 min, and stored on ice prior to analysis by high-performance liquid chromatography (HPLC).

**MiaE Activity Assay.** For the MiaE enzyme assays using an *in vitro* electron transport chain (ETC), solutions of $i^6A$-$ACSL^{Trp}$ were prepared following MiaA reaction at selected concentrations (3−60 μM) for steady-state experiments. To each solution were added MiaE, Fd, and FdR, reaching final concentrations of 0.5, 4, and 4 μM, respectively. Reactions were initiated by addition of 500 μM NADPH. Sample aliquots were collected at different time periods (1−5 min), heat-denatured at 95 °C for 2 min, and then placed in ice prior to being analyzed by HPLC. For free nucleoside substrate kinetics, samples of the synthetic isopentenylated adenosine ($i^6A$) were prepared (0.5−5.0 mM) under conditions identical to those described above for $i^6A$-ACSL reactions.

**HPLC Sample Preparation.** Free nucleosides were generated from modified RNA oligonucleotides for HPLC analysis following methods previously published.[23,43] Sample aliquots (60 μL) containing RNA oligomers were treated with 5 μL of 10 mM $ZnSO_4$ and 10 μL of nuclease P1 [200 units/mL, in 30 mM sodium acetate buffer (pH 5.4)] and incubated for 16 h at 37 °C to cleave the RNA oligomer into its constitutive nucleotides. Following cleavage, 10 μL of 0.5 M Tris buffer (pH 8.3) and 10 μL of bacterial alkaline phosphatase (BAP) (100 units/mL, in 2.5 M ammonium sulfate) were added and allowed to incubate for an additional 2 h at 37 °C to remove the nucleotide 5′-phosphate group. The resulting nucleoside solutions were then filtered through a 0.22 μm Spin-X centrifuge tube (Costar) prior to HPLC analysis.

**HPLC Analysis.** A Shimadzu quaternary pump liquid chromatograph (LC-20AD XR/LC 30AD) was equipped with a photodiode array detector (SPD-M20A). The column was a Phenomenex, Gemini-NH 3 μm, C18 110 Å, 150 cm × 4.6 mm column. The mobile phase consisted of (A) 2.5% methanol in 0.01 M $NH_4H_2PO_4$ (pH 5.3), (B) 20% methanol in 0.01 M $NH_4H_2PO_4$ (pH 5.1), and (C) 35% acetonitrile in 0.01 M $NH_4H_2PO_4$ (pH 4.9). The injection volume was 20 μL and the flow rate 1 mL/min. The column temperature was 25 °C. UV−visible detection was monitored at 266 nm ($\lambda_{max}$ of $i^6A$) and 272 nm ($\lambda_{max}$ of $io^6A$). The concentrations of $i^6A$ (retention time, 67.3 min) and *E*-$io^6A$ (retention time, 55.5 min) were determined by comparison to standard calibration curves (0.01−5 mM) produced from synthetic standards.[23]

**Liquid Chromatography−Tandem Mass Spectrometry (LC−MS/MS) and Data Analysis.** Verification of the enzymatic product was performed by multiple-reaction monitoring (MRM) using a triple-quadrupole LC−MS/MS instrument (Shimadzu Scientific Instruments, LCMS 8040).[44] The molecular ions ($M^+$) of the enzyme substrate ($i^6A$, $m/z$ 336) and product ($io^6A$, $m/z$ 352) were selected for secondary fragmentation. MRM optimization was then employed to maximize transition intensity and sensitivity for each fragment, allowing for quantitation of product ions. The optimized MRM method was used to verify both substrate and product by direct injection of enzymatic assays. These results were compared to those of direct injection of synthetic standards.

**EPR/Mössbauer Sample Preparation.** Reduced EPR samples were prepared inside the anaerobic glovebox (Coy Laboratory Products Inc.) by addition of a stoichiometric sodium dithionite solution (30 mM) mediated with methyl viologen. Dithionite solutions were prepared fresh and calibrated as described elsewhere.[23] For ACSL titrations, a 1 mM stock solution of $ACSL^{Trp}$ was added (0−95 μL) via a Hamilton 100 μL gastight syringe to 180 μL of 350 μM reduced MiaE in a 1.0 mL Eppendorf microfuge tube. Following additions of $ACSL^{Trp}$, anaerobic buffer was used to dilute samples to a final volume of 275 μL, resulting in a final MiaE concentration of 230 μM. EPR samples were then allowed to equilibrate on ice for 15 min prior to being transferred into a 4 mm quartz EPR tube (707-SQ-250MM, Wilmad-Lab Glass) with a 250 μL Hamilton gastight syringe equipped with a 6 in. needle. Finally, EPR tubes were frozen slowly in liquid $N_2$ under anaerobic conditions prior to analysis. Mössbauer samples were prepared under identical anaerobic conditions and reduced (if necessary) as described for EPR samples. All samples were prepared from a stock solution of 1.9 mM $^{57}$Fe-enriched enzyme. Aliquots were taken from the enzyme stock (250 μL), reduced (if necessary), and then diluted with anaerobic buffer to obtain equivalent 500 μL samples of 960 μM $^{57}$Fe-MiaE (oxidized and reduced). Samples of the $ACSL^{Trp}$−MiaE complex were prepared by mixing 240 μL of 1.9 mM $^{57}$Fe-MiaE with 260 μL of a 2.6 mM $ACSL^{Trp}$ stock solution to obtain a final $ACSL^{Trp}$:MiaE molar ratio of 1.5:1.0.

**Spectroscopy.** *UV−Visible Spectroscopy.* All UV−visible measurements were performed on an Agilent (Santa Clara, CA) 8453 photo diode array spectrometer. Measurements were taken in ES quartz cuvettes (NSG Precision Cells, Farmingdale, NY).

*Circular Dichroism (CD).* All CD experiments were performed on a JASCO 715 UV−visible circular dichroism spectrometer with a xenon arc light source. Unless otherwise stated, protein samples analyzed by CD were prepared in 10 mM sodium phosphate buffer (pH 8.0) filtered through a 0.22 μm polypropylene membrane filter (VWR international). Equine heart myoglobin (CAS Registry No. 100684-32-0), chicken egg white lysozyme (CAS Registry No. 12650-88-3),


DOI: 10.1021/bi5012207
*Biochemistry* 2015, 54, 363−376

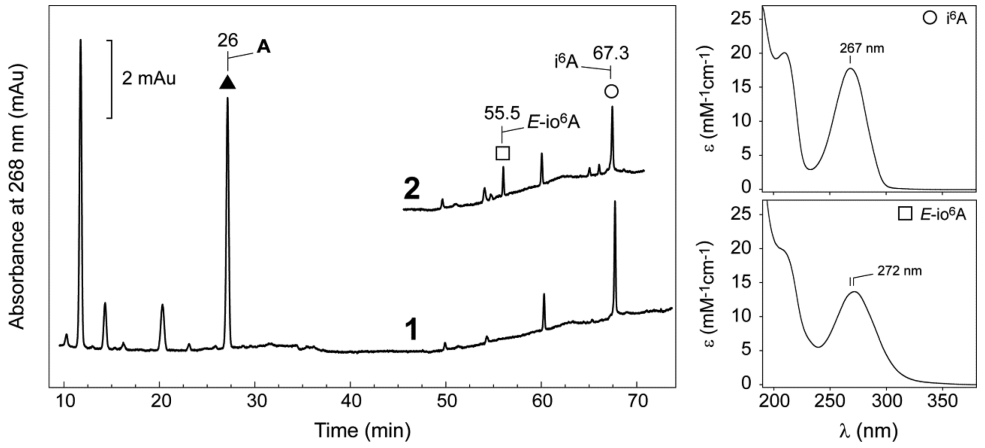


**Figure 1.** Representative HPLC chromatograms (left) of i$^6$A and io$^6$A nucleosides in MiaA and MiaE reactions (analytes detected spectrophotometrically at 268 nm). Chromatogram 1 shows the i$^6$A peak (○, 67.3 min) produced by the reaction of ACSL with enzyme MiaA in the presence of excess DMAPP. Remaining adenosine (A) is also observed (▲, 26 min). Chromatogram 2 shows the product of the reaction of i$^6$A-ACSL with MiaE (□, *E*-io$^6$A produced at 55.5 min). UV−vis absorption spectra (right) of synthetic i$^6$A and *E*-io$^6$A standards.

and poly-L-lysine (CAS Registry No. 25988-63-0) purchased from Sigma-Aldrich were used as standards for secondary structure determination as described elsewhere.[45] CD results were also interpreted using the freely available online software K2D3 (http://k2d3.ogic.ca/). Far-UV (185−300 nm) CD spectra of protein were recorded in a quartz cuvette with a path length of 0.1 cm and a volume of ~0.45 mL at a scan speed of 40 nm/min at ambient temperature. In a typical CD experiment, 5 $\mu$L of 450 $\mu$M MiaE enzyme was added to 445 $\mu$L of buffer to yield a final concentration of 5 $\mu$M in the cuvette. In RNA binding experiments, MiaE (5 $\mu$M) was titrated with an increasing concentration of ACSL RNA oligomers (0−2 molar equiv). Stock solutions of the RNA oligomer were prepared at 500 $\mu$M such that RNA additions did not significantly dilute the sample or alter the buffer composition. All spectra were signal-averaged ($n$ = 3) for noise reduction.

*Analysis of CD Titration Data.* The normalized change in ellipticity ($\Delta\theta$) was fit using a single-site equilibrium binding model (eq 1), which assumes reversible binding of substrate (A) and enzyme (E) to produce a substrate-bound complex (EA). The concentration of each species can be described by eqs 2 and 3 and solved for EA in terms of [E$_t$], [A$_t$], and $K$ to yield eq 4. Because both [E$_t$] and [A$_t$] are known, the concentration of EA is dependent only on $K$, which is determined by nonlinear least-squares fitting to eq 4. For the sake of simplicity, the binding constant ($K_D$) is substituted for $1/K$ in eq 4.

$$K = [EA]/([E_f][A_f]) \tag{1}$$

$$[E_t] = [E_f] + EA \tag{2}$$

$$[A_t] = [A_f] + EA \tag{3}$$

$$[EA] = \frac{[A_t] + [E_t] + 1/K \pm \sqrt{([A_t] + [E_t] + 1/K)^2 - 4[A_t][E_t]}}{2} \tag{4}$$

*EPR Spectroscopy.* X-Band (9 GHz) EPR spectra were recorded on a Bruker (Billerica, MA) EMX Plus spectrometer equipped with a bimodal resonator (Bruker model 4116DM). Low-temperature measurements were taken using an Oxford ESR900 cryostat and an Oxford ITC 503 temperature controller. A modulation frequency of 100 kHz was used for all EPR spectra. All experimental data used for spin quantitation were collected under nonsaturating conditions as verified by half-power microwave saturation ($P_{1/2}$). EPR spectra of reduced MiaE were simulated by diagonalization of the spin Hamiltonian (eq 5) using SpinCount version 5.3.5190.24657 (created by M. P. Hendrich, Carnegie Mellon University, Pittsburgh, PA). Here, $J$ is the exchange coupling constant between the two ferrous iron sites ($S_1 = S_2 = 2$), **g** is the **g** tensor, and the axial and rhombic zero-field splitting parameters are represented by $D$ and $E$, respectively.[46]

$$\hat{H} = -2J(\mathbf{S_1}\cdot\mathbf{S_2}) + \sum_{i=1}^{2}[D_i(\hat{S}_{zi}^{\,2} - 2) + E_i(\hat{S}_{xi}^{\,2} - \hat{S}_{yi}^{\,2}) + \beta_e\mathbf{S}_i\cdot\mathbf{g}_i\cdot\mathbf{B}] \tag{5}$$

This equation simplifies under the assumption that the energy of the exchange coupling constant ($J$) is comparable to (or larger than) the zero-field splitting ($D$) of the diferrous cluster. Under this constraint, the $S$ = 4 Hamiltonian takes the form illustrated in eq 6.

$$\mathbf{D}\left(\hat{S}_z^{\,2} - \frac{\hat{S}^2}{3}\right) + \mathbf{E}(\hat{S}_x^{\,2} - \hat{S}_y^{\,2}) + \beta_e\mathbf{S}\cdot\mathbf{g}\cdot\mathbf{B} \tag{6}$$

This program computes the powder pattern for a uniform spherical distribution of the magnetic field vector **B**, and the transition intensities are calculated using "Fermi's golden rule".[47] The simulations are generated considering all intensity factors, both theoretical and experimental. The concentration of species can be used as a constraint during spectral simulation, which allows quantitative determination of the concentration by comparison of the experimental and simulated signal intensities.[48] The only unknown factor relating the spin concentration to signal intensity is an instrumental factor that depends on the microwave detection system. This factor is determined using a Cu(II)EDTA spin standard.[49,23]

The half-power microwave saturation ($P_{1/2}$) for reduced MiaE as a function of ACSL$^{Trp}$ concentration was determined using the SpinCount software package according to eq 7.



DOI: 10.1021/bi5012207
*Biochemistry* 2015, 54, 363−376

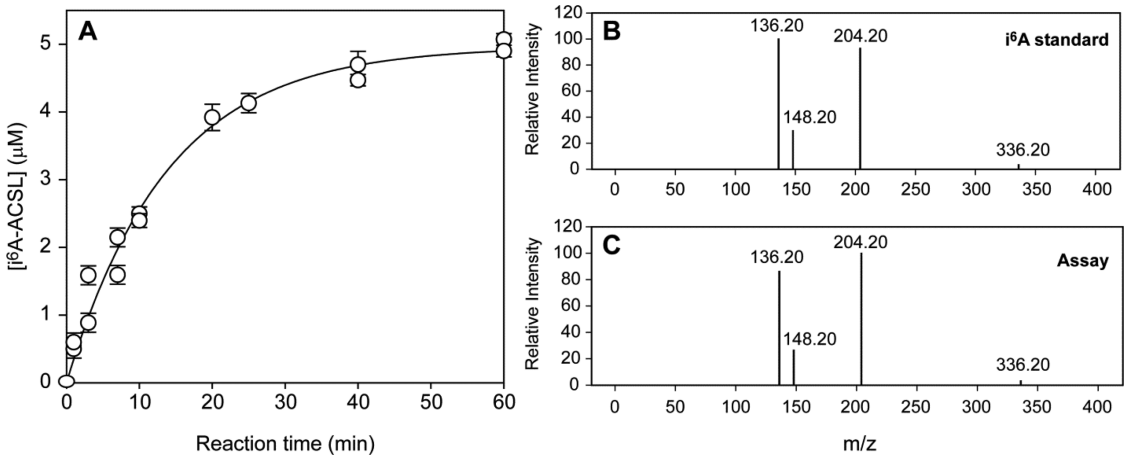


**Figure 2.** (A) Rate of MiaA-catalyzed $N^6$-isopentenyladenosine ACSL formation ($i^6A_{37}$-ACSL) as observed by reversed phase HPLC. Accumulation of $i^6$A-ACSL was best fit by a single exponential with a $k_{obs}$ of $(1.1 \pm 0.1) \times 10^{-3}$ $s^{-1}$ and an $A$ of $4.94 \pm 0.03$ $\mu$M. Assay conditions: 200 nM MiaA, 100 $\mu$M DMAPP, 100 $\mu$g of BSA, 60 mM Tris-HCl, 20 mM $MgCl_2$, 2 mM DTT, pH 7.5, and 37 °C. LC−MS/MS spectra of MRM transitions of designated $i^6$A product ions are shown within the right panels for comparison. Panel B corresponds to the $i^6$A synthetic standard, and panel C illustrates the direct injection of the enzymatic product.

$$S/\sqrt{P} = \frac{A}{(1 + P/P_{1/2})^{b/2}} \quad (7)$$

The software performs least-squares fitting of the normalized derivative signal intensity ($S$) as a function of the microwave power ($P$). $A$ represents the normalized maximal signal amplitude. The variable $b$ is a spectroscopic inhomogeneity factor that is characteristic of the spin packet of the observed resonance. Generally, the signal packet derived from frozen solutions and powders exhibits inhomogeneous line broadening behavior ($b = 1$).

*Mössbauer Spectroscopy.* Mössbauer spectra for $^{57}$Fe-incorporated resting and reduced MiaE were collected at 4 K on a model MS4 WRC spectrometer equipped with a closed loop cryostat system (SEE Co., Edina, MN) as described elsewhere.[50] Spectral fitting was performed using SpinCount.

## RESULTS

**Enzymatic Assays.** To evaluate the steady-state kinetics of MiaE $i^6$A hydroxylation, isopentenylated RNA oligomers were first enzymatically synthesized using recombinant MiaA. It has been reported that the minimal substrate for bacterial MiaA is the anticodon stem loop (ACSL) of targeted tRNA molecules;[42] therefore, a 17-nucleotide oligomer corresponding to the ACSL region of $tRNA^{Trp}$ ($^{27}$CCGGUCUCCAAAAC-CG$^{43}$G, designated $ACSL^{Trp}$ henceforth) was selected as a starting substrate for enzymatic assays. The activities of recombinant *S. typhimurium* MiaA and MiaE were monitored using the reverse phase HPLC method. As illustrated in the HPLC chromatogram (Figure 1, trace 1), addition of 200 nM MiaA to a buffered solution containing $ACSL^{Trp}$ (5.6 $\mu$M) and excess DMAPP (100 $\mu$M) results in the formation of a peak at 67.3 min (○). This new peak matches the retention time, UV−visible absorption features, and mass spectra (described below) of the synthetic $i^6$A nucleoside standard. Figure 2A shows the rate of $i^6$A-$ACSL^{Trp}$ production for duplicate MiaA-catalyzed reactions over 1 h. The amplitude of $i^6$A product formation upon completion of the reaction ($A = 4.94 \pm 0.03$ $\mu$M) and the pseudo-first-order rate constant [$k_{obs} = (1.1 \pm 0.1) \times 10^{-3}$ $s^{-1}$] were determined from the best fit. Along with the rate of $i^6$A-$ACSL^{Trp}$ formation observed at 67.3 min (Figure 1), a concomitant decrease in the adenosine peak area (▲, 26 min) can be observed (data not shown). The initial rate of this reaction can be obtained from the product amplitude and the pseudo-first-order rate constant ($v_0 = k_{obs}A$); thus, the enzyme (MiaA)-normalized initial rate ($v_0$/[E]) for $i^6$A-ACSL formation is $0.028 \pm 0.004$ $s^{-1}$. The observed change in amplitude of $i^6$A formation of the single-exponential phase accounts for ~88% of the expected stoichiometry for MiaA-catalyzed ACSL isopentenylation. Therefore, under these conditions, nearly complete formation of $i^6$-$ACSL^{Trp}$ is observed within 1 h at ambient temperature.

Confirmation of the MiaA product identity was verified using LC−MS/MS by MRM. In positive ion mode, the $i^6$A parent ion $[M + H]^+$ is observed at $m/z$ 336.2. Secondary fragmentation of the parent ion produces secondary ions at $m/z$ 136.2, 148.2, and 204.2 corresponding to adenine, $N^6$-methyladenine, and $N^6$-isopentenyladenine, respectively.[51] As illustrated in panels B and C of Figure 2, direct injection of the $i^6$A synthetic standard and enzymatic assay produced identical fragmentation patterns. The top panel (Figure 2B) represents the MRM mass spectrum (molecular ion at $m/z$ 336) observed for the $i^6$A nucleoside. For comparison, panel C shows the mass spectrum obtained by direct injection of MiaA enzymatic assays. Given the matching fragmentation pattern and relative intensities obtained for the MiaA product, we can conclude that the product generated within MiaA is indeed the $i^6$A-$ACSL^{Trp}$.

Previously, the peroxide-shunt-catalyzed rates of hydroxylation were reported for MiaE using three synthetic $\beta$-nucleoside substrates [2-thiomethyl-$N^6$-(3-methyl-2-butenylamino)-adenosine ($ms^2i^6A$), $N^6$-(3-methyl-2-butenylamino)adenosine ($i^6A$), and 2-chloro-$N^6$-(3-methyl-2-butenylamino)adenosine ($Cl^2i^6A$)].[23] While the peroxide-shunt pathway removes the need for an external electron source, such reactions are frequently slower and exhibit chemo- and stereoselectivity decreased compared to those of reactions utilizing a functional electron transport chain. Therefore, to improve our understanding of the physiologically relevant MiaE catalytic system, a functional electron transport chain was constructed on the basis of what has worked previously with the soluble stearoyl-ACP $\Delta^9$-desaturase.[29,52,53] In these reactions, NADPH serves as the electron source and ferredoxin reductase (FdR) and ferredoxin


DOI: 10.1021/bi5012207
*Biochemistry* 2015, 54, 363−376

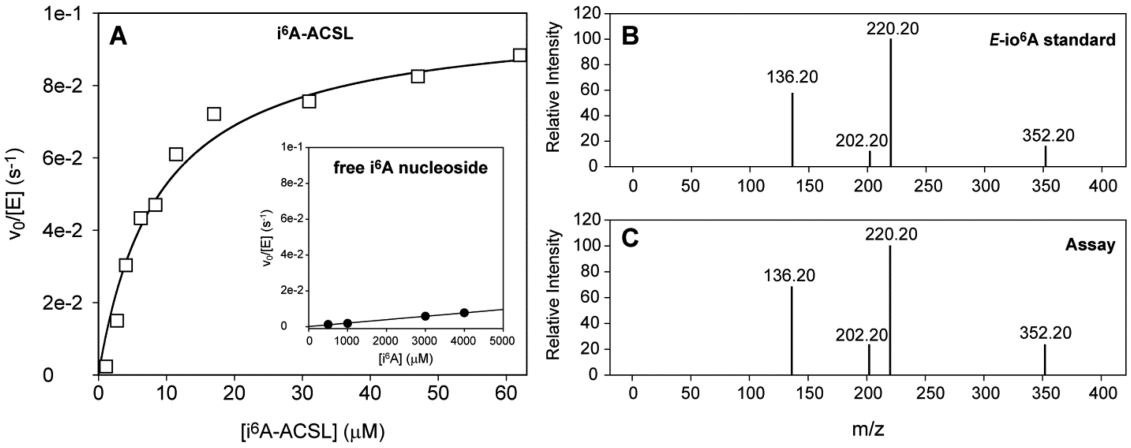


**Figure 3.** (A) Steady-state kinetics for MiaE-catalyzed hydroxylation of i$^6$A-ACSL$^{Trp}$ compared to that of the free i$^6$A nucleoside (inset). The Michaelis–Menten parameters $k_{cat}$, $K_M$, and $V/K$ determined by best fit are 0.10 ± 0.01 $s^{-1}$, 9.1 ± 1.5 $\mu$M, and ~11000 $M^{-1}$ $s^{-1}$, respectively. Although full saturation is not observed for the MiaE-catalyzed hydroxylation of the free i$^6$A nucleoside, the pseudo-second-order rate constant (approximately $k_{cat}/K_m$) can be determined from the slope of the line (1.9 ± 0.1 $M^{-1}$ $s^{-1}$). Assay conditions: 0.5 $\mu$M MiaE, 4 $\mu$M Fd, 4 $\mu$M FdR, 500 $\mu$M NADPH, pH 7.5, and 37 °C. LC–MS/MS spectra of MRM transitions of designated *E*-io$^6$A product ions are shown within the right panels for comparison. Panel B corresponds to the *E*-io$^6$A synthetic standard and panel C to the direct injection of enzymatic product.

(Fd) provide an electron transport chain (ETC) to shuttle electrons from NADPH to the diiron active site of MiaE. In a typical reaction, the i$^6$A-ACSL$^{Trp}$ substrate is generated using recombinant MiaA as described above. Prior to initiation of the MiaE reaction, the concentration of i$^6$A-ACSL$^{Trp}$ produced is verified by HPLC as described in Materials and Methods. Substrate i$^6$A-ACSL solutions were generated at concentrations ranging from 0 to 60 $\mu$M. To these solutions were added purified MiaE, Fd, and FdR, and reactions were initiated by addition of 500 $\mu$M NADPH. At selected time points, aliquots were quenched by heat denaturation and worked up for HPLC analysis. A representative HPLC chromatogram for illustrating the *E*-io$^6$A peak (55.5 min) is shown in Figure 1 (trace 2). Confirmation of the MiaE product and stereochemistry was performed as previously described.[23] As with peroxide-shunt assays reported previously, the product of (Fd/FdR)–ETC steady-state assays retains nearly stoichiometric (>98%) *E* stereoselectivity.

In contrast to what was previously observed in peroxide-shunt assays,[23] the initial rate of MiaE-catalyzed i$^6$A-ACSL$^{Trp}$ hydroxylation utilizing the *in vitro* (Fd/FdR)–ETC assay follows typical saturation kinetics as illustrated in Figure 3. The Michaelis–Menten parameters, $k_{cat}$, $K_M$, and $V/K$, determined by best fit are 0.10 ± 0.01 $s^{-1}$, 9.1 ± 1.5 $\mu$M, and ~11000 $M^{-1}$ $s^{-1}$, respectively. LC–MS/MS analyses (MRM transitions) of the *E*-io$^6$A standard and MiaE product are shown in panels B and C of Figure 3, respectively. As expected for a monooxygenase reaction, the molecular ion ($M^+$ = $m/z$ 352.2) observed for the MiaE-hydroxylated product is increased by $m/z$ 16 relative to that of the i$^6$A substrate (Figure 2; $M^+$ = $m/z$ 336.2). Secondary fragmentation of the parent ion produces peaks at $m/z$ 136.2, 202.2, and 220.2. The $m/z$ 220.2 peak is assigned to an $N^6$-(4-hydroxyisopentenyl)adenine ion on the basis of the $m/z$ +16 shift observed relative to i$^6$A, whereas the $m/z$ 136.2 and 202.2 peaks are assigned to adenine and $N^6$-(4-methylbutadiene)adenine fragmentation ions.[51] To the best of our knowledge, this represents the first instance of steady-state kinetic values reported for any MiaE enzyme.

While vastly slower, the MiaE-catalyzed hydroxylation of the free i$^6$A nucleoside can also be observed using the (Fd/FdR)–ETC steady-state assay. As shown in the inset of Figure 3A, full substrate saturation of MiaE is never observed within the solubility limit of the nucleoside (~5 mM). This same behavior was observed in peroxide-shunt assays, as well.[23] From the slope of the line, the pseudo-second-order rate constant (approximately $k_{cat}/K_m$) can be determined (1.9 ± 0.1 $M^{-1}$ $s^{-1}$). By comparison to the $V/K$ determined for i$^6$A-ACSL$^{Trp}$ substrates, a nearly 6000-fold increase in enzymatic efficiency is imparted by reaction mixtures containing the 17-nucleotide i$^6$A-ACSL$^{Trp}$ as compared to the free i$^6$A nucleoside.

**CD Spectroscopy.** The impact of substrate tRNA–MiaE interactions on secondary structure was investigated by CD spectroscopy. Because the RNA oligomers utilized lack the i$^6$A modificaiton, these experiments are designed to investigate the extent to which the RNA secondary structure influences enzyme recognition. As illustrated in Figure 4A (spectrum 1),

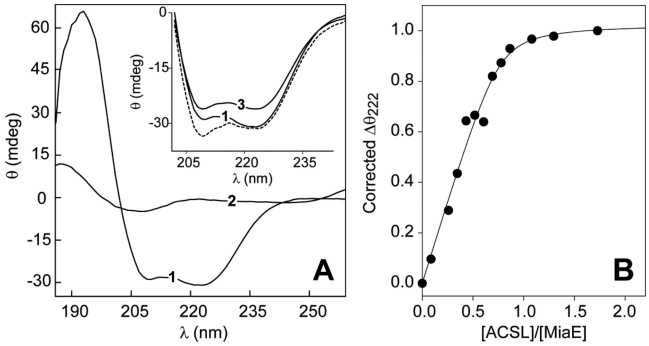


**Figure 4.** (A) Circular dichroism spectra of 5 $\mu$M as-isolated MiaE (trace 1) and 5 $\mu$M ACSL$^{Trp}$ (trace 2). Within the inset is a replot of the observed CD spectra for an equimolar complex of oxidized MiaE and ACSL$^{Trp}$ (trace 3) compared to that of the resting enzyme. Assuming no change in the secondary structure of MiaE or ACSL$^{Trp}$, the expected CD spectra should be the sum of traces 1 and 2 (---). Panel B shows the results obtained from titration of the RNA oligomer into a sample of as-isolated MiaE. Assuming a single-binding site equilibrium model, these data could be fit to eq 4 (—) to obtain the binding constant for the MiaE–ACSL$^{Trp}$ complex. A description of control experiments, data analysis, and fitting is provided in Figures S1–S3 of the Supporting Information.



DOI: 10.1021/bi5012207
*Biochemistry* 2015, 54, 363–376

the UV CD spectra (185−260 nm) of resting MiaE show a maximum at 193 nm and two minima at 208 and 222 nm. These features are fairly typical of proteins with high $\alpha$-helical content. Analysis of the MiaE secondary structure was made by comparison to known protein standards (myoglobin, poly-L-lysine, and lysozyme) as described in Materials and Methods. From this analysis, it was determined that the resting MiaE $\alpha$-helical content was 78 ± 5%.

At an equivalent molar concentration relative to MiaE (5 $\mu$M), the RNA helical and hairpin loop secondary structure of ACSL$^{Trp}$ (Figure 4A, trace 2) contributes to the CD response within this spectral window. While these features are small relative to the protein response, additional controls are needed to ensure that any spectral changes observed are not simply due to nonspecific interactions or contributions from the RNA CD spectra.

In the absence of any interactions between the ACSL$^{Trp}$ RNA oligomer and resting MiaE, the expected CD spectra for an equimolar mixture of MiaE and ACSL$^{Trp}$ would be the sum of each spectral contribution (1 + 2). As illustrated in Figure 4A (inset), the observed spectrum for the MiaE−RNA complex (trace 3) is significantly different from either that of the initial resting MiaE (trace 1) or the sum of CD spectra [1 + 2 (dashed line)]. This result indicates that RNA binding induces a change in the secondary structure within the MiaE−RNA complex. To be clear, it is not possible to resolve if the spectral shift observed is solely due to protein or RNA conformational changes. In all likelihood, it reflects a change in the secondary structure of both molecules upon complexation.

Native tRNA molecules all exhibit a defined hairpin loop secondary structure within the ACSL region. It is therefore reasonable to speculate that this structural motif may be important for MiaE substrate recognition. To test this hypothesis, a 10-nucleotide RNA oligomer incapable of forming a hairpin loop (termed ssRNA) was added to samples of resting MiaE. While this oligomer is shorter than the 17-nucleotide ACSL$^{Trp}$ sequence, it is important to recognize that formation of the hairpin loop decreases the head−tail length of ACSL$^{Trp}$ by nearly 2-fold. Thus, the ssRNA sequence lacking this structural motif should be similar in length to ACSL$^{Trp}$. Indeed, CD spectroscopy confirms the absence of any secondary structure within the ssRNA oligomer. Regardless, no change in the secondary structure of the MiaE−RNA complex is observed by CD (or EPR) spectroscopy in these experiments (Figure S3 of the Supporting Information). This observation suggests that the conformational change induced by complexation of MiaE with ACSL$^{Trp}$ cannot be attributed to nonspecific interactions with single-stranded RNA. The synthetic nucleosides (ms$^2$i$^6$A, i$^6$A, and Cl$^2$i$^6$A) represent the simplest possible substrates for MiaE in both peroxide-shunt and biological electron transfer (Fd/FdR)−ETC assays. As these substrates are unable to elicit a similar conformational change upon addition to resting MiaE (Figure S3 of the Supporting Information), the observed conformational change within the MiaE active site cannot be triggered by a single protein−nucleoside interaction either. On the basis of these experiments, it is reasonable to conclude that the tRNA hairpin loop is a critical point of interaction between MiaE and its tRNA substrates.

As noted earlier, the RNA secondary structure contributes to the observed CD spectra within the UV region. These contributions become significant at elevated RNA oligomer concentrations, and thus, they need to be subtracted from the collected data. Figure S1A of the Supporting Information shows a series of stacked CD spectra for resting MiaE (5 $\mu$M) titrated with increasing molar equivalents of ACSL$^{Trp}$. For each spectrum collected, the signal attributed to free ACSL$^{Trp}$ (trace 2) was scaled for molar concentration and then subtracted from each spectrum collected. The resulting difference spectra shown in Figure S1B of the Supporting Information were then used to follow formation of the MiaE−ACSL$^{Trp}$ complex in titration experiments. Within the difference spectra, the absence of the broad absorptive feature ($\lambda$ = 270 nm) unique to RNA spectra is consistent with the removal of signals associated with unbound ACSL$^{Trp}$. As shown in Figure S1B of the Supporting Information, addition of ACSL$^{Trp}$ to a sample of resting MiaE results in a small but detectable positive shift in the ellipticity at 222 nm ($\Delta\theta_{222}$). At 1 molar equiv (ACSL$^{Trp}$:MiaE), this signal shift is small relative to the total protein signal (~4 mdeg at 5 $\mu$M MiaE) but is readily detectable. No further changes are observed at this wavelength at titration points beyond 1 molar equiv. Figure 4B illustrates the normalized $\Delta\theta_{222}$ plotted as a function of ACSL$^{Trp}$ molar equivalents. These results indicate that a single mole of ACSL$^{Trp}$ binds to MiaE to yield a 1:1 stoichiometric complex. Assuming reversible binding of ACSL$^{Trp}$ to MiaE, the normalized change in ellipticity can be fit using eq 4 to determine the binding constant for ACSL$^{Trp}$ ($K_d$ = 0.3 ± 0.3 $\mu$M). It should be noted that the value of the binding constant determined from these fits is dependent on the concentration of enzyme utilized in CD titrations. Unfortunately, instrumental signal noise becomes increasingly problematic at protein concentrations below ~3 $\mu$M, and thus, these CD experiments are unable to resolve binding affinities below this value ($K_d \leq 3$ $\mu$M). As a result, the $K_d$ values determined from CD data fits are likely significantly overestimated. Thus, while CD spectroscopy is ideally suited to observe a conformational change in the MiaE−RNA complex, more sensitive techniques are needed to accurately evaluate the actual substrate binding affinities for MiaE.

An additional point to consider is whether the oxidation state of the MiaE diiron site influences the protein secondary structure or RNA binding affinity. As indicated by Figure S2 of the Supporting Information, no difference is observed in the secondary structure of MiaE upon reduction. Furthermore, addition of 1 molar equiv of ACSL$^{Trp}$ to either form results in identical changes in ellipticity. Titration experiments performed using anaerobic reduced enzyme reveal no significant deviation in the apparent ACSL$^{Trp}$ binding affinity. While it is likely that the binding affinities differ somewhat between the oxidized and reduced enzyme, CD spectroscopy does not have the sensitivity to detect such differences.

**EPR Spectroscopy.** The diferrous active site of MiaE can be probed by parallel mode X-band EPR spectroscopy. As previously reported, the temperature dependence, intensity, line width, and $g$ values of this signal are similar to those reported for the reduced diiron sites within several other bacterial non-heme monooxygenase enzymes (DpmLNO, T4MOH, and MMOH).[23,54] This feature is attributed to the weak ferromagnetic exchange coupling between two high-spin ferrous sites ($S_1 = S_2 = 2$), resulting in a ground-state $S$ = 4 spin manifold. The reduced MiaE signal deviates from Curie law behavior in that the temperature dependence of the $g \sim 16$ temperature-normalized signal intensity (S×T) decreases with increasing temperature (Figure S5 of the Supporting Information). The maximal intensity for this signal is observed at 4.2 K and completely vanishes by 25 K. This indicates that


DOI: 10.1021/bi5012207
Biochemistry 2015, 54, 363−376

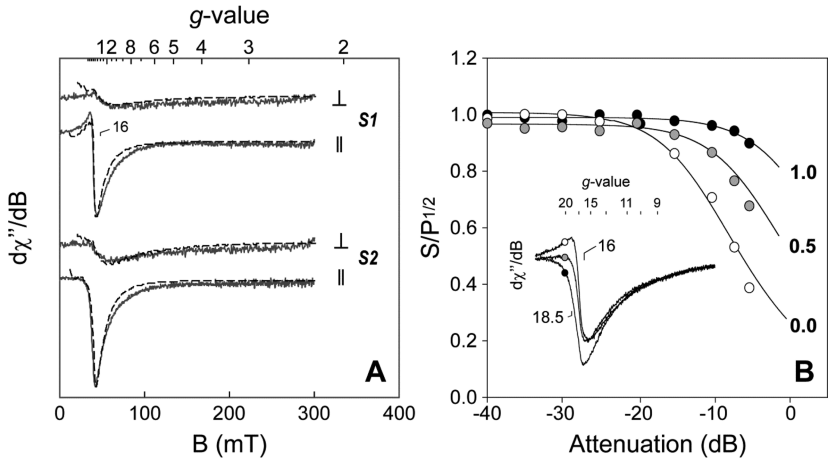


**Figure 5.** (A) X-Band perpendicular (⊥) and parallel mode (||) EPR spectra of reduced MiaE (**1**) and MiaE precomplexed with 1.5 molar equiv of $ACSL^{Trp}$ (**2**). EPR simulations (---) are overlaid on the spectra for comparison. Instrumental parameters: microwave frequency, 9.644 GHz (⊥) and 9.375 GHz (||); modulation amplitude, 0.92 mT; temperature, 4.2 K. EPR simulation parameters. ***S1***: $S = 4$, $g_y = 2.011$; $D = 1.0$ cm$^{-1}$; $E/D = 0.19$; $\sigma_D = 0.02$ cm$^{-1}$; $\sigma_{E/D} = 0.15$; $\sigma_B = 1.2$ mT; 0.22 mM ***S1***. ***S2***: $S = 4$, $g_y = 2.010$; $D = 1.0$ cm$^{-1}$; $E/D = 0.11$; $\sigma_D = 0.10$ cm$^{-1}$; $\sigma_{E/D} = 0.08$; $\sigma_B = 1.3$ mT; 0.24 mM ***S2***. (B) Parallel mode $g \sim 16$ signal half-saturation microwave power ($P_{1/2}$) for reduced MiaE precomplexed with 0 ($P_{1/2} = 15$ mW), 0.5 ($P_{1/2} = 76$ mW), and 1.0 molar equiv ($P_{1/2} = 300$ mW) of $ACSL^{Trp}$.

this transition must originate from a ground doublet within the lowest-lying spin manifold of a non-Kramers system.

Similar ACSL titrations like those described above for CD experiments were performed on reduced diferrous MiaE and followed by dual-mode X-band EPR spectroscopy. As indicated in Figure 5A, the line shape for the reduced MiaE (**1**) $g \sim 16$ signal is significantly altered when MiaE is precomplexed with 1.5 molar equiv of $ACSL^{Trp}$. Furthermore, Figure 5B demonstrates that the extent of change observed in the $g \sim 16$ signal is directly proportional to the amount of $ACSL^{Trp}$ added up to 1 molar equiv. Addition of $ACSL^{Trp}$ beyond 1 molar equivalent has no further effect on the observed $g \sim 16$ EPR spectra of reduced MiaE. In addition to the obvious spectral changes illustrated, $ACSL^{Trp}$ binding also significantly increases the microwave power needed for half-saturation ($P_{1/2}$) of the $g \sim 16$ signal (Figure 5B). As with CD experiments, addition of the ssRNA sequence had no effect on the observed EPR spectrum for reduced MiaE (Figure S3 of the Supporting Information). This shift in the $g \sim 16$ parallel mode EPR signal upon binding of tRNA to reduced MiaE is very reminiscent of what has been reported for bacterial multicomponent diiron monooxygenases upon titration with their corresponding effector proteins.[26,27,29,33,41,42] This also suggests that MiaE may be an excellent model system for studying protein−effector interactions and their impact on diiron site geometry and reactivity.

As described in Materials and Methods, EPR simulations (Figure 5, dashed lines) of the reduced diiron cluster can be generated with the assumption that the magnitude of the ferromagnetic exchange coupling constant ($J$) is comparable to or larger than the zero-field splitting term ($D$) ($|J| \geq D$).[23] Under this constraint, the temperature dependence of the $g \sim 16$ EPR signal becomes solely a function of the axial zero-field splitting term ($D$). This value can be determined experimentally by fitting the temperature-normalized signal area (S×T) to a Boltzmann population distribution for an isolated $S = 4$ manifold. Once the $D$ value is obtained for each signal, the general spin Hamiltonian can be used to calculate correct EPR transition probabilities.[23,55,56] As illustrated in Figure S5 of the Supporting Information, both reduced MiaE and MiaE precomplexed with 1.5 molar equiv of $ACSL^{Trp}$ exhibit nearly identical temperature dependence. Both data sets are fit assuming a transition within the ground doublet (levels 1 and 2) of an $S = 4$ spin manifold to obtain an axial zero-field splitting of $D = 1.0 \pm 0.2$ cm$^{-1}$.

X-Band EPR spectral simulations were calculated using the experimentally derived zero-field splitting term for both perpendicular and parallel mode frequency polarizations and overlaid on the observed spectra. As shown in Figure 5, both X-band perpendicular and parallel mode EPR spectra for reduced MiaE (**1**) and MiaE precomplexed with 1.5 mol equiv of $ACSL^{Trp}$ (**2**) can be reasonably simulated using the parameters described in the legend of Figure 5. From these simulations, the spin concentration determined for ***S1*** and ***S2*** are 222 $\mu$M (97%) and 240 $\mu$M (105%), respectively.

In the previous EPR spectroscopic characterization of reduced MiaE, the spin quantitation determined by EPR simulation of reduced MiaE was low relative to the expected value (44% relative to the total iron).[23] For the sake of simplicity, these initial calculations did not account for any intrinsic anisotropy of the diiron **g** tensor ($g_{x,y,z} \sim 2.0$). However, parallel mode signals are largely influenced by a single $g$ value within the spin system ($g_y$ in this instance). This value was allowed to vary over a reasonable limit for ferrous iron ($2.00 < g_y < 2.15$) while the observed spectra were fit. Essentially stoichiometric quantitation of the reduced MiaE active site is calculated in the overlaid simulation (***S1***) that utilizes the zero-field splitting parameters ($D = 1.0$ cm$^{-1}$; $E/D = 0.19$). The line width and sigal intensity for this signal are dominated by distributions in $D$ and $E/D$ ($\sigma_D$ and $\sigma_{E/D}$, respectively). By comparison, the ACSL-bound MiaE simulation (***S2***) suggests that substrate binding alters the coordination geometry of the reduced active site. While the value of the axial zero-field splitting term remains constant, a significant decrease is observed in the rhombicity ($E/D = 0.11$) calculated for the reduced diiron cluster. For the sake of clarity, all spectroscopic parameters used for ***S1*** and ***S2*** simulations are provided in the legend of Figure 5.

The dual-mode EPR simulations accurately reflect the signal intensity (and thus concentration) of each species (**1** and **2**) in



DOI: 10.1021/bi5012207
*Biochemistry* 2015, 54, 363−376

both perpendicular and parallel mode; however, significant approximations ($|J| \geq D$) were made to limit the number of independent variables necessary for calculations. Complete validation of simulations would require additional dual-mode EPR characterization at additional frequencies. In lieu of this, Mössbauer spectroscopy was used to independently corroborate results obtained in EPR spectroscopic experiments and refine UV−visible molar extinction coefficient determinations for this enzyme.

**Table 1. Observed Mössbauer Parameters for MiaE and the ACSL$^{Trp}$−MiaE Complex**

| description | site | $\delta$ (mm/s) | $\Delta E_Q$ (mm/s) | $\Gamma$ | % |
|---|---|---|---|---|---|
| ($Fe^{II}Fe^{II}$)-MiaE | 1 | 1.19 | 2.86 | 0.57 | 48 |
| | 2 | 1.32 | 3.12 | 0.40 | 48 |
| ($Fe^{II}Fe^{II}$)-MiaE with ACSL | 1 | 1.19 | 2.79 | 0.54 | 46 |
| | 2 | 1.33 | 3.07 | 0.40 | 46 |
| ($Fe^{III}Fe^{III}$)-MiaE | 1 | 0.50 | 0.65 | 0.30 | 15 |
| | 2 | 0.53 | 1.57 | 0.30 | 42 |
| | 3 | 0.49 | 2.20 | 0.30 | 42 |
| ($Fe^{III}Fe^{III}$)-MiaE with ACSL | 1 | 0.51 | 0.66 | 0.35 | 22 |
| | 2 | 0.53 | 1.55 | 0.30 | 39 |
| | 3 | 0.48 | 2.20 | 0.30 | 39 |

**Mössbauer Spectroscopy.** As illustrated in Figure 6, the Mössbauer spectra (A) for the resting diferric enzyme exhibit three sets of quadrupole doublets designated [**1**], [**2**], and [**3**]. The two nested doublets [**2**] [$\delta_2$ = 0.53(1) and $\Delta E_Q$ = 1.57(2) mm/s] and [**3**] [$\delta_3$ = 0.49(1), and $\Delta E_Q$ = 2.20(2) mm/s] are in equal concentrations and collectively represent 84(2)% of the total Fe in the sample. This observation suggests two possibilities (i) The majority of the resting MiaE cluster is composed of a single binuclear species containing inequivalent iron sites, or (ii) two distinct populations of diferric clusters with equivalent iron centers are present within resting MiaE. Unlike most non-heme diiron proteins, MiaE exhibits a monomeric protein configuration. Thus, only one diiron cluster is present per enzyme. As the relative proportions of major doublets [**2**] and [**3**] are always equivalent (1:1) across multiple preparations (oxidized and reduced), it is highly unlikely that these doublets represent two distinct populations of the resting MiaE cluster in chemical equilibrium. Similar behavior has been reported for the diferric active site of hemerythrin, as well as a variety of non-heme diiron model complexes.[57−59] The larger $\Delta E_Q$ values observed for species [**2**] and [**3**] are quite similar to those reported for the $\mu$-oxo-bridged diferric clusters in Δ9D and the small subunit of ribonucleotide reductase (R2).[60,61] For comparison, Mössbauer parameters reported for a variety of enzymatic and model diiron site are listed in Table S1 of the Supporting Information. The remaining doublet [**1**] [$\delta_1$ = 0.50(1), and $\Delta E_Q$ = 0.65(1) mm/s] contributes ∼15(3)% to the total Fe. The smaller quadrupole splitting observed for [**1**] is consistent with what has been observed for $\mu$-hydroxo-bridged diferric sites within MMOH and T4MOH.[54,62] It is therefore reasonable that this doublet originates from a small fraction of MiaE containing a diferric iron site bridged by a $\mu$-hydroxo ligand.

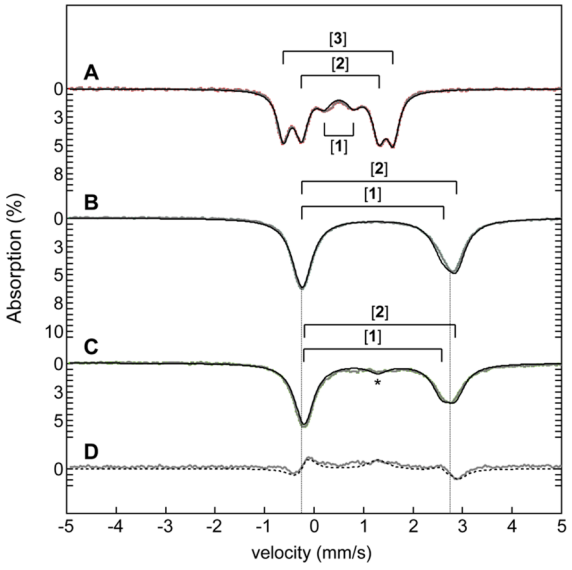


**Figure 6.** Selected Mössbauer spectra of resting diferric (A) and reduced MiaE enzyme (B). Sample conditions: 500 $\mu$L of 960 $\mu$M $^{57}$Fe-incorporated MiaE, 20 mM HEPES, 100 mM NaCl, pH 8.0. (C) Reduced MiaE precomplexed with 1.5 molar equiv of ACSL$^{Trp}$. Spectral fits (solid black line) are overlaid on the data for the sake of clarity. The shift in the doublets observed upon addition of ACSL$^{Trp}$ to the reduced enzyme is indicated by the vertical dotted line. The difference spectrum (B − C) and difference fit (---) are provided in trace D. The feature designated with an asterisk is attributed to a trace amount of oxidized MiaE (∼10 ± 5%). The Mössbauer parameters used to simulate each spectrum are listed in Table 1.

While the relative proportions of these species ([**1**], [**2**], and [**3**]) differ, the Mössbauer parameters observed here are consistent with what has been previously reported for the resting MiaE enzyme with one exception.[16] In the previous characterization, EPR, Mössbauer, and HYSCORE spectroscopic measurements involving resting MiaE, an appreciable fraction (∼30%) of the MiaE diiron site was observed as a mixed valent $Fe^{II}$−$Fe^{III}$ cluster.[16] In contrast to this observation, no mixed valent species could be detected by either EPR or Mössbauer spectroscopy in the samples prepared here.

The Mössbauer spectrum for MiaE reduced by sodium dithionite and methyl viologen is shown in Figure 6B. This spectrum is best fit to two unresolved quadrupole doublets [**1**] [$\delta_1$ = 1.19(3), and $\Delta E_Q$ = 2.86(3) mm/s] and [**2**] [$\delta_2$ = 1.32(3), and $\Delta E_Q$ = 3.12(3) mm/s]. As with the oxidized doublets, reduced doublets [**1**] and [**2**] contribute an equal proportion to the overall spectrum, collectively accounting for 96(4)% of the total Fe in the sample. Both the isomer shift and quadrupole splitting observed for reduced MiaE are similar to those reported for a variety of reduced non-heme diiron centers (Table S1 of the Supporting Information). The equal contribution of each ferrous doublet [**1**] and [**2**] suggests that the individual Fe sites within the cluster remain inequivalent following reduction of the enzyme.

As indicated by Figure 6C, no significant variance is observed in the isomer shift of the two doublets [**1**] and [**2**] upon addition of a 1.5-fold molar excess of ACSL$^{Trp}$ to reduced MiaE. This result is expected as isomer shifts are dominated by the oxidation state of the Fe sites. By contrast, the quadrupole splitting for each doublet is noticeably decreased [$\Delta E_Q$ values of 2.79(2) and 3.07(2) mm/s, respectively] upon addition of ACSL$^{Trp}$. This effect is demonstrated by the difference spectra (B − C) illustrated in Figure 6D. This observation agrees well with the change in the zero-field splitting parameters ($D$ and $E/D$) demonstrated by EPR spectroscopy. The effect of addition of ACSL$^{Trp}$ was also measured in the resting diferric enzyme,


DOI: 10.1021/bi5012207
Biochemistry 2015, 54, 363−376

but other than a slight deviation (~5%) in the composition of the $\mu$-hydroxo doublet [**1**], both $\delta$ and $\Delta E_Q$ observed for doublets [**2**] and [**3**] were unaffected upon addition of ACSL$^{Trp}$.

## DISCUSSION

As with peroxide-shunt assays,[23] the product of steady-state assays utilizing the Fd/FdR electron transport chain retains essentially stoichiometric (98%) *E* stereoselectivity. In contrast to peroxide-shunt and (Fd/FdR)−ETC assays utilizing a single nucleoside, substrate saturation kinetics is observed for only the i$^6$A-ACSL$^{Trp}$ substrate ($k_{cat}$ = 0.10 ± 0.01 s$^{-1}$, and $K_M$ = 9.1 ± 1.5 $\mu$M). To the best of our knowledge, this represents the first instance of steady-state kinetic values reported for any tRNA-monooxygenase. While the $k_{cat}$ of MiaE is slow compared to those of typical metabolic enzymes (1−10$^6$ s$^{-1}$), this value is similar to what has been observed for enzymes involved in modifying genomic DNA (0.1−1.0 s$^{-1}$).[63] In such enzymes, it has been postulated that the slow reaction rates impart greater accuracy. The experiments described here demonstrate a protein conformational change upon binding of tRNA to MiaE that influences the electronic structure of the diiron site. Moreover, a ~6000-fold increase in catalytic efficiency is observed for the RNA i$^6$A-ACSL$^{Trp}$ substrate compared to that of the free i$^6$A nucleoside. While much of this increased activity can be attributed to increased binding affinity, spectroscopic results suggest that tRNA binding may provide an activating event in this enzyme, and perhaps related enzymes.

Although synthetic nucleosides (ms$^2$i$^6$A, i$^6$A, and Cl$^2$i$^6$A) represent the simplest possible substrates for MiaE in both peroxide-shunt and (Fd/FdR)−ETC assays,[23] they do not elicit the same conformational change upon addition to MiaE as observed by CD spectroscopy. Furthermore, the single-stranded RNA oligomer lacking the ability to form a hairpin loop also had no observable effect on either CD or EPR spectra. Taken together, it is reasonable to conclude that the tRNA hairpin loop is a critical point of interaction between MiaE and its tRNA substrates. If a protein structure similar to that observed for other non-heme diiron enzymes is assumed, the diiron cluster of MiaE is likely buried within the interior of a four-helix bundle.[22,64] Therefore, the spectroscopic perturbations witnessed by both EPR and Mössbauer spectroscopy upon addition of ACSL$^{Trp}$ are unlikely to reflect direct coordination of the RNA oligomer to the active site. Instead, tRNA binding likely results in a protein conformational change in the MiaE structure, which imparts a shift in the diiron active site geometry.

To first-order, validation of EPR spectral simulations can be taken from the accuracy of active site spin quantitation for the reduced MiaE (***S1***) and the reduced MiaE−ACSL$^{Trp}$ complex (***S2***). On the basis of these calculations, the MiaE protein conformational change observed by CD spectroscopy is conferred to the MiaE active site, resulting in a perturbation to the zero-field splitting parameter ($E/D$) of the reduced diiron cluster. Another possibility is that ACSL$^{Trp}$ binding alters the exchange coupling ($J$) of the cluster. The simulations provided here assume an isolated $S$ = 4 spin manifold and thus are insensitive to this parameter. The increased half-saturation microwave power observed for ***S2*** ($P_{1/2}$ = 300 mW) compared to that of ***S1*** ($P_{1/2}$ = 15 mW) indicates faster electronic relaxation rates for ***S2***. Potentially, this could be the result of increased $m_s$ eigenstate mixing within the spin manifold; however, it is not immediately clear if this effect is attributed to changes in the magnitude of the exchange coupling ($J$) or rhombicity ($E/D$); potentially, it could be a mixture of both. Regardless, the observed substrate-gated conformational change in the reduced diiron active site alters the geometric configuration of the diiron site, which may in turn alter the $Fe^{II/III}$ redox potential and/or the $O_2$ reactivity of the substrate-bound enzyme. As the simulations provided here utilize a very simplistic model of the reduced diiron site, the zero-field splitting values reported by simulation should not be considered analytical determinations of these values. Further investigation is necessary to analytically determine the exact impact of this interaction on the active site electronic structure.

On the basis of the small quadrupole splitting ($\Delta E_Q$ = 0.65), the ferric doublet [**1**] shown in Figure 6 (spectra A) is assigned as a set of equivalent Fe sites bridged by a $\mu$-hydroxo ligand. Similar ($\mu$-hydroxo) doublets have been reported from Mössbauer analysis of as-isolated and reduced Δ9D,[62] T4MOH,[54] and DpmLNO.[55] All known non-heme diiron enzymes containing a $\mu$-hydroxy-bridged diiron cluster lack Fe-associated absorption bands.[54] By this reasoning, the population of MiaE protein containing a $\mu$-hydroxy-bridged diferric cluster is not expected to contribute to the observed Fe-associated ligand to metal charge transfer bands within the UV−visible spectrum. Because the molar extinction coefficient previously reported ($\varepsilon_{370}$ = 5100 ± 700 M$^{-1}$ cm$^{-1}$) for resting MiaE was determined on the basis of total iron content, this value is under-reported.[23] By subtraction of the fraction of $\mu$-hydroxo-bridged MiaE determined by Mössbauer spectroscopy from the concentration of resting MiaE, a corrected molar extinction coefficient can be obtained that is specific to the resting Fe-oxo LMCT at pH 8.0 ($\varepsilon_{370}$ = 5800 ± 700 M$^{-1}$ cm$^{-1}$).

The larger $\Delta E_Q$ observed for resting MiaE doublets [**1**] and [**2**] (spectra A) is more consistent with $\mu$-oxo-bridged diferric clusters (Table S1 of the Supporting Information). The 1:1 contribution of doublets [**2**] and [**3**] within the resting MiaE cluster implies that the iron coordination environment for each site is inequivalent. A number of structural factors could give rise to this behavior, for example, an asymmetric coordination of carboxylate or histidine ligands surrounding each iron site or potentially a terminal hydroxo ligand at one Fe site. At this point, the exact structural factors giving rise to this inequivalence have yet to be determined.

In agreement with EPR experiments, addition of excess ACSL$^{Trp}$ RNA oligomer to samples of reduced MiaE yields a small but detectable shift (0.05−0.07 mm/s) in the observed $\Delta E_Q$ for doublets [**2**] and [**3**] relative to that of the free reduced enzyme. No effect was observed on the isomer shift ($\delta$) of either the oxidized or reduced enzyme. While the ACSL-induced active site perturbation is not as pronounced in Mössbauer experiments, the EPR signal intensity and line shape of integer spin signals are largely dependent on the rhombicity ($E/D$) of the system.[56] Therefore, EPR can frequently be more sensitive to subtle geometric perturbations at the active site as compared to Mössbauer spectroscopy. Regardless, both techniques demonstrate that ACSL$^{Trp}$ binding imparts a conformational change within the reduced MiaE active site.

CD experiments indicate that protein/RNA conformational changes within the MiaE−ACSL complex are unaffected by the diiron site oxidation state. In apparent contrast to this observation, Mössbauer spectral perturbations are observed only for binding of ACSL$^{Trp}$ to the reduced enzyme. This may suggest that active site conformational changes occur only in


DOI: 10.1021/bi5012207
*Biochemistry* 2015, 54, 363−376

the reduced cluster. However, because $\Delta E_Q$ values are 1.4−1.8-fold larger in magnitude for the reduced iron sites than for the ferric iron sites, a more likely explanation is that these subtle shifts are simply unresolved within the oxidized enzyme.

Nearly all non-heme diiron monooxygenase enzymes exhibit a multimeric quaternary structure. This raises the possibility of interprotomer communication and potential for "half-sites" reactivity.[29−32] Such factors significantly complicate functional characterization for this class of enzymes. A more practical consideration when dealing with multimeric enzymes is that the active site located within one protomer is spectroscopically indistinguishable from an active site on an adjacent protomer. This generates an inherent ambiguity in assigning spectroscopic features. Thus, despite a wealth of mechanistic and structural studies of non-heme diiron enzymes, to date our fundamental understanding of how the protein environment modulates the reactivity of the diiron cluster remains somewhat superficial. In this respect, MiaE represents an unprecedented opportunity to study a minimal non-heme diiron catalytic system in the absence of any potential for interprotomer cooperativity. This work provides an important first step in the identification of key intermolecular interactions involved in MiaE-catalyzed tRNA hydroxylation. Nevertheless, additional studies are needed to fully model the structural factors influencing the enzymatic reactivity, tRNA specificity, and impact of tRNA binding on the active site reactivity and electronic structure of MiaE.

The spectroscopic shifts observed for MiaE upon $ACSL^{Trp}$ binding are reminiscent of the effects reported for bacterial multicomponent diiron monooxygenases upon addition of their corresponding effector proteins. As the changes observed in the integer-spin EPR signal of the reduced diiron active site are not observed upon addition of the free nucleoside substrate ($i^6A$) or ssRNA sequences, it can be inferred that tRNA substrates behave as their own effector molecules for MiaE. To date, this has not been previously reported for any other member of the non-heme diiron monooxygenase family. These observations also imply that substrate−enzyme interactions could play a pivotal role in modulating the reactivity of the MiaE diiron active site. Indeed, beyond the obvious increase in the expected binding affinity for ACSL substrates relative to free nucleoside substrates, it is tempting to speculate that the vastly increased activity toward RNA substrates is due to an activating event within the MiaE active site upon substrate binding.

## ■ ASSOCIATED CONTENT

### Supporting Information

Raw CD results for ACSL titrations, comparison of ACSL binding for oxidized and reduced MiaE, temperature dependence of X-band EPR, reduced MiaE $g \sim 16$ signals, and a table of representative UV−visible/Mössbauer properties reported for non-heme diiron enzymes and model complexes. This material is available free of charge via the Internet at http://pubs.acs.org.

## ■ AUTHOR INFORMATION


### Corresponding Author

*Department of Chemistry and Biochemistry, 700 Planetarium Place, Room 130, The University of Texas at Arlington, Arlington, TX 76019. E-mail: bspierce@uta.edu. Phone: (817) 272-9066. Fax: (817) 272-3808.



### Funding

This work was supported by start-up funds provided by the University of Texas at Arlington, Department of Chemistry and Biochemistry. We also acknowledge National Science Foundation financial support (CRIF:MU CHE-0840509) for the purchase of the JEOL ECA500 500 MHz FT-NMR spectrometers.


### Notes

The authors declare no competing financial interest.

## ■ ACKNOWLEDGMENTS


We acknowledge the University of Texas at Arlington (UTA) Shimadzu Center for Advanced Analytical Chemistry (UTA) for the use of HPLC and LC−MS/MS instrumentation and the UTA Center for Nanostructured Materials (http://www.uta.edu/cos/cnm/) for the use of EPR facilities. We also thank Professor Paul Lindahl and Mrinmoy Chakrabarti [Texas A&M University, College Station, TX (National Institutes of Health Grant GM084266)] for their generous assistance in collecting Mössbauer spectra for MiaE.


## ■ REFERENCES


(1) Gustilo, E. M., Vendeix, F. A. P., and Agris, P. F. (2008) tRNA's modifications bring order to gene expression. *Curr. Opin. Microbiol. 11*, 134−140.

(2) Björk, G. R., Durand, J. M., Hagervall, T. G., Leipuviene, R., Lundgren, H. K., Nilsson, K., Chen, P., Qian, Q., and Urbonavicius, J. (1999) Transfer RNA modification: Influence on translational frameshifting and metabolism. *FEBS Lett. 452*, 47−51.

(3) Cabello-Villegas, J., Winkler, M. E., and Nikonowicz, E. P. (2002) Solution Conformations of Unmodified and $A_{37}$ $N^6$-dimethylallyl Modified Anticodon Stem-loops of *Escherichia coli* $tRNA^{Phe}$. *J. Mol. Biol. 319*, 1015−1034.

(4) Persson, B. C. (1993) Modification of tRNA as a regulatory device. *Mol. Microbiol. 8*, 1011−1016.

(5) Yonath, A. (2005) Antibiotics Targeting Ribosomes: Resistance, Selectivity, Synergism, and Cellular Regulation. *Annu. Rev. Biochem. 74*, 649−679.

(6) Abbink, T. E. M., and Berkhout, B. (2008) HIV-1 reverse transcription initiation: A potential target for novel antivirals? *Virus Res. 134*, 4−18.

(7) Ju, J., Jiang, J., and Fesler, A. (2013) miRNA: The new frontier in cancer medicine. *Future Med. Chem. 5*, 983−985.

(8) Wu, J., Liu, S., Yu, J., Zhou, G., Rao, D., Jay, C. M., Kumar, P., Sanchez, R., Templeton, N., Senzer, N., Maples, P., Nemunaitis, J., and Brunicardi, F. C. (2014) Vertically integrated translational studies of PDX1 as a therapeutic target for pancreatic cancer via a novel bifunctional RNAi platform. *Cancer Gene Ther. 21*, 48−53.

(9) Persson, B. C., Olafsson, O., Lundgren, H. K., Hederstedt, L., and Björk, G. R. (1998) The $ms^2io^6A37$ modification of tRNA in *Salmonella typhimurium* regulates growth on citric acid cycle intermediates. *J. Bacteriol. 180*, 3144−3151.

(10) Petersson, L., Gräslund, A., Ehrenberg, A., Sjöberg, B. M., and Reichard, P. (1980) The iron center in ribonucleotide reductase from *Escherichia coli*. *J. Biol. Chem. 255*, 6706−6712.

(11) Moore, J. A., and Poulter, C. D. (1997) *Escherichia coli* dimethylallyl diphosphate:tRNA dimethylallyltransferase: A binding mechanism for recombinant enzyme. *Biochemistry 36*, 604−614.

(12) Anton, B. P., Russell, S. P., Vertrees, J., Kasif, S., Raleigh, E. A., Limbach, P. A., and Roberts, R. J. (2010) Functional characterization of the YmcB and YqeV tRNA methylthiotransferases of *Bacillus subtilis*. *Nucleic Acids Res. 38*, 6195−6205.

(13) Pierrel, F., Douki, T., Fontecave, M., and Atta, M. (2004) MiaB Protein is a bifunctional radical-S-adenosylmethionine enzyme involved in thiolation and methylation of tRNA. *J. Biol. Chem. 279*, 47555−47563.




DOI: 10.1021/bi5012207
*Biochemistry* 2015, 54, 363−376

(14) Arragain, S., Handelman, S. K., Forouhar, F., Wei, F.-Y., Tomizawa, K., Hunt, J. F., Douki, T., Fontecave, M., Mulliez, E., and Atta, M. (2010) Identification of Eukaryotic and Prokaryotic Methylthiotransferase for Biosynthesis of 2-Methylthio-N6-threonylcarbamoyladenosine in tRNA. *J. Biol. Chem. 285*, 28425−28433.
(15) Björk, G. R., Ericson, J. U., Gustafsson, C. E. D., Hagervall, T. G., Jonsson, Y. H., and Wikstrom, P. M. (1987) Transfer RNA modification. *Annu. Rev. Biochem. 56*, 263−285.
(16) Mathevon, C., Pierrel, F., Oddou, J. L., Garcia-Serres, R., Blondin, G., Latour, J. M., Menage, S., Gambarelli, S., Fontecave, M., and Atta, M. (2007) tRNA-modifying MiaE protein from *Salmonella typhimurium* is a nonheme diiron monooxygenase. *Proc. Natl. Acad. Sci. U.S.A. 104*, 13295−13300.
(17) Esberg, B., Leung, H.-C. E., Tsui, H.-C. T., Björk, G. R., and Winkler, M. E. (1999) Identification of the *miaB* Gene, Involved in Methylthiolation of Isopentenylated $A_{37}$ Derivatives in the tRNA of *Salmonella typhimurium* and *Escherichia coli*. *J. Bacteriol. 181*, 7256−7265.
(18) Buck, M., and Ames, B. N. (1984) A modified nucleotide in tRNA as a possible regulator of aerobiosis: Synthesis of cis-2-methylthioribosylzeatin in the tRNA of *Salmonella*. *Cell 36*, 523−531.
(19) Esberg, B., and Björk, G. R. (1995) The methylthio group ($ms^2$) of $N^6$-(4-hydroxyisopentenyl)-2-methylthioadenosine ($ms^2io^6A$) present next to the anticodon contributes to the decoding efficiency of the tRNA. *J. Bacteriol. 177*, 1967−1975.
(20) Ajitkumar, P., and Cherayil, J. D. (1985) Presence of 2-methylthioribosyl-trans-zeatin in *Azotobacter vinelandii* tRNA. *J. Bacteriol. 162*, 752−755.
(21) Durand, J. M., Björk, G. R., Kuwae, A., Yoshikawa, M., and Sasakawa, C. (1997) The modified nucleoside 2-methylthio-$N^6$-isopentenyladenosine in tRNA of *Shigella flexneri* is required for expression of virulence genes. *J. Bacteriol. 179*, 5777−5782.
(22) Kaminska, K. H., Baraniak, U., Boniecki, M., Nowaczyk, K., Czerwoniec, A., and Bujnicki, J. M. (2008) Structural bioinformatics analysis of enzymes involved in the biosynthesis pathway of the hypermodified nucleoside $ms^2io^6A_{37}$ in tRNA. *Proteins 70*, 1−18.
(23) Corder, A. L., Subedi, B. P., Zhang, S., Dark, A. M., Foss, F. W., and Pierce, B. S. (2013) Peroxide-Shunt Substrate-Specificity for the *Salmonella typhimurium* $O_2$-Dependent tRNA Modifying Monooxygenase (MiaE). *Biochemistry 52*, 6182−6196.
(24) Feig, A. L., and Lippard, S. (1994) Reactions of non-heme iron(II) centers with dioxygen in biology and chemistry. *Chem. Rev. 94*, 759−805.
(25) Wallar, B. J., and Lipscomb, J. D. (1996) Dioxygen activation by enzymes containing binuclear non-heme iron clusters. *Chem. Rev. 96*, 2625−2658.
(26) Solomon, E. I., Decker, A., and Lehnert, N. (2003) Non-heme iron enzymes: Contrasts to heme catalysis. *Proc. Natl. Acad. Sci. U.S.A. 100*, 3589−3594.
(27) Lei, Q. P., Cui, X., Kurtz, D. M., Amster, I. J., Chernushevich, I. V., and Standing, K. G. (1998) Electrospray mass spectrometry studies of non-heme iron-containing proteins. *Anal. Chem. 70*, 1838−1846.
(28) Notomista, E., Lahm, A., Di Donato, A., and Tramontano, A. (2003) Evolution of Bacterial and Archaeal multicomponent monooxygenases. *J. Mol. Evol. 56*, 435−445.
(29) Broadwater, J. A., Ai, J., Loehr, T. M., Sanders-Loehr, J., and Fox, B. G. (1998) Peroxodiferric intermediate of stearoyl-acyl carrier protein $\Delta^9$-desaturase: Oxidase reactivity during single turnover and implications for the mechanism of desaturation. *Biochemistry 37*, 14664−14671.
(30) Sjöberg, B. M., Karlsson, M., and Jornvall, H. (1987) Half-site reactivity of the tyrosyl radical of ribonucleotide reductase from *Escherichia coli*. *J. Biol. Chem. 262*, 9736−9743.
(31) Ge, J., Perlstein, D. L., Nguyen, H. H., Bar, G., Griffin, R. G., and Stubbe, J. (2001) Why multiple small subunits (Y2 and Y4) for yeast ribonucleotide reductase? Toward understanding the role of Y4. *Proc. Natl. Acad. Sci. U.S.A. 98*, 10067−10072.
(32) Sommerhalter, M., Voegtli, W. C., Perlstein, D. L., Ge, J., Stubbe, J., and Rosenzweig, A. C. (2004) Structures of the yeast ribonucleotide reducatase Rnr2 and Rnr4 homodimers. *Biochemistry 43*, 7736−7742.
(33) Lyle, K. S., Haas, J. A., and Fox, B. G. (2003) Rapid-Mix and Chemical Quench Studies of Ferredoxin-Reduced Stearoyl-Acyl Carrier Protein Desaturase. *Biochemistry 42*, 5857−5866.
(34) Baik, M. H., Newcomb, M., Friesner, R. A., and Lippard, S. J. (2003) Mechanistic studies on the hydroxylation of methane by methane monooxygenase. *Chem. Rev. 103*, 2385−2419.
(35) Bailey, L. J., and Fox, B. G. (2009) Crystallographic and catalytic studies of the peroxide-shunt reaction in a diiron hydroxylase. *Biochemistry 48*, 8932−8939.
(36) Froland, W. A., Andersson, K. K., Lee, S.-K., Liu, Y., and Lipscomb, J. D. (1992) Methane Monooxygenase Component B and Reductase Alter the Regioselectivity of the Hydroxylase Component-catalyzed Reactions. *J. Biol. Chem. 267*, 17588−17597.
(37) Murray, L. J., and Lippard, S. J. (2007) Substrate trafficking and dioxygen activation in bacterial multicomponent monooxygenases. *Acc. Chem. Res. 40*, 466−474.
(38) Sazinsky, M. H., and Lippard, S. J. (2006) Correlating Structure with Function in Bacterial Multicomponent Monooxygenases and Related Diiron Proteins. *Acc. Chem. Res. 39*, 558−566.
(39) Mitchell, K. H., Studts, J. M., and Fox, B. G. (2002) Combined Participation of Hydroxylase Active Site Residues and Effector Protein Binding in a Para to Ortho Modulation of Toluene 4-Monooxygenase Regiospecificity. *Biochemistry 41*, 3176−3188.
(40) Cheng, H., Westler, W. M., Xia, B., Oh, B. H., and Markley, J. L. (1995) Protein expression, selective isotopic labeling, and analysis of hyperfine-shifted NMR signals of *Anabaena* 7120 vegetative [2Fe-2S]ferredoxin. *Arch. Biochem. Biophys. 316*, 619−634.
(41) Hoffman, B. J., Broadwater, J. A., Johnson, P., Harper, J., Fox, B. G., and Kenealy, W. R. (1995) Lactose fed-batch overexpression of recombinant metalloproteins in *Escherichia coli* BL21 (DE3): Process control yielding high levels of metal-incorporated, soluble protein. *Protein Expression Purif. 6*, 646−654.
(42) Leung, H. C., Chen, Y., and Winkler, M. E. (1997) Regulation of substrate recognition by the MiaA tRNA prenyltransferase modification enzyme of *Escherichia coli* K-12. *J. Biol. Chem. 272*, 13073−13083.
(43) Gehrke, C. W., and Kuo, K. C. (1989) Ribonucleoside Analysis by Reversed-Phase High-Performance Liquid-Chromatography. *J. Chromatogr. 471*, 3−36.
(44) Yost, R. A., and Fetterolf, D. D. (1983) Tandem mass spectrometry (MS/MS) instrumentation. *Mass Spectrom. Rev. 2*, 1−45.
(45) Greenfield, N. J. (2007) Using circular dichroism spectra to estimate protein secondary structure. *Nat. Protoc. 1*, 2876−2890.
(46) Abragam, A., and Bleaney, B. (1970) *Electron paramagnetic resonance of transition ions*, Oxford University Press, New York.
(47) Cohen-Tannoudji, C., Diu, B., and Laloë, F. (1977) *Quantum mechanics*, Vol. *II*, John Wiley & Sons, New York.
(48) Hendrich, M. P., Petasis, D., Arciero, D. M., and Hooper, A. B. (2001) Correlations of structure and electronic properties from EPR spectroscopy of hydroxylamine oxidoreductase. *J. Am. Chem. Soc. 123*, 2997−3005.
(49) Weil, J. A., Bolton, J. R., and Wertz, J. E. (1993) *Electron paramagnetic resonance: Elementary theory and practical applications*, John Wiley & Sons, Inc., New York.
(50) Cockrell, A., McCormick, S. P., Moore, M. J., Chakrabarti, M., and Lindahl, P. A. (2014) Mössbauer, EPR, and Modeling Study of Iron Trafficking and Regulation in Δccc1 and CCC1-up *Saccharomyces cerevisiae*. *Biochemistry 53*, 2926−2940.
(51) Shaw, S. J., Desiderio, D. M., Tsuboyama, K., and McCloskey, J. A. (1970) Mass spectrometry of nucleic acid components. Analogs of adenosine. *J. Am. Chem. Soc. 92*, 2510−2522.
(52) Haas, J. A., and Fox, B. G. (1999) Role of hydrophobic partitioning in substrate selectivity and turnover of the *Ricinus communis* stearoyl acyl carrier protein $\Delta^9$-desaturase. *Biochemistry 38*, 12833−12840.


DOI: 10.1021/bi5012207
*Biochemistry* 2015, 54, 363−376

(53) Lyle, K. S., Haas, J. A., and Fox, B. G. (2003) Rapid-mix and chemical quench studies of ferredoxin-reduced stearoyl-acyl carrier protein desaturase. *Biochemistry 42*, 5857−5866.
(54) Pikus, J. D., Studts, J. M., Achim, C., Kauffmann, K. E., Münck, E., Steffan, R. J., McClay, K., and Fox, B. G. (1996) Recombinant toluene-4-monooxygenase: Catalytic and Mössbauer studies of the purified diiron and Rieske components of a four-protein complex. *Biochemistry 35*, 9106−9119.
(55) Cadieux, E., Vrajmasu, V., Achim, C., Powlowski, J., and Münck, E. (2002) Biochemical, Mössbauer, and EPR studies of the diiron cluster of phenol hydroxylase from *Pseudomonas* sp. strain CF 600. *Biochemistry 41*, 10680−10691.
(56) Hendrich, M. P., and Debrunner, P. G. (1989) Integer-spin electron paramagnetic resonance of iron proteins. *Biophys. J. 56*, 489−506.
(57) LeCloux, D. D., Barrios, A. M., Mizoguchi, T. J., and Lippard, S. J. (1998) Modeling the Diiron Centers of Non-Heme Iron Enzymes. Preparation of Sterically Hindered Diiron(II) Tetracarboxylate Complexes and Their Reactions with Dioxygen. *J. Am. Chem. Soc. 120*, 9001−9014.
(58) Fox, B. G., Shanklin, J., Somerville, C., and Münck, E. (1993) Stearoyl-acyl carrier protein $\Delta^9$-desaturase from *Ricinus communis* is a diiron-oxo protein. *Proc. Natl. Acad. Sci. U.S.A. 90*, 2486−2490.
(59) Clark, P. E., and Webb, J. (1981) Mössbauer spectroscopic studies of hemerythrin from *Phascolosoma lurco* (syn. *Phascolosoma Arcuatum*). *Biochemistry 20*, 4628−4632.
(60) Lynch, J. B., Juarez-Garcia, C., Münck, E., and Que, L. (1989) Mössbauer and EPR studies of the binuclear iron center in ribonucleotide reductase from *Escherichia coli*. A new iron-to-protein stoichiometry. *J. Biol. Chem. 264*, 8091−8096.
(61) Shu, L. J., Broadwater, J. A., Achim, C., Fox, B. G., Münck, E., and Que, L. (1998) EXAFS and Mössbauer characterization of the diiron(III) site in stearoyl-acyl carrier protein $\Delta^9$-desaturase. *JBIC, J. Biol. Inorg. Chem. 3*, 392−400.
(62) Fox, B. G., Hendrich, M. P., Surerus, K. K., Andersson, K. K., Froland, W. A., Lipscomb, J. D., and Münck, E. (1993) Mössbauer, EPR, and ENDOR studies of the hydroxylase and reductase components of methane monooxygenase from *Methylosinus trichosporium* OB3b. *J. Am. Chem. Soc. 115*, 3688−3701.
(63) Traut, T. (2008) The Limits for Life Define the Limits for Enzymes. *Allosteric Regulatory Enzymes*, Chapter 2, Springer, New York.
(64) Joint Center for Structural Genomics (2006) The crystal structure of putative tRNA-($ms^2io^6A$)-hydroxylase (NP_744337.1) from *Pseudomonas putida* KT2440 at 2.05 Å resolution. PDB entry 2ITB.


DOI: 10.1021/bi5012207
*Biochemistry* 2015, 54, 363−376